cultured cells. Our findings are consistent with potential links between chronic subacute inflammation and insulin resistance (*26*, *27*), whether this is mediated by TNF-α produced in fat (*28*–*31*) or through TNF-α–independent mechanisms. As a potentially important example of the latter, in rodent muscle, FFA infusion activates PKC-θ (*32*), a known activator of IKK (*33*), and FFA-induced insulin resistance is suppressed by aspirin treatment and in *Ikkβ*$^{+/-}$ mice (*34*). IKK activation through any mechanism initiates NF-κB–mediated transcription, which in certain cells would enhance the production of TNF-α. This positive feedback loop could perpetuate a vicious cycle of low-level inflammatory signaling, leading to insulin resistance. Our findings predict that IKK inhibition breaks this cycle. Too few tools are currently available to treat patients with insulin resistance and type 2 diabetes; IKKβ may provide a valuable target for the discovery of new drugs to treat these conditions.

References and Notes

1. E. Kopp, S. Ghosh, *Science* **265**, 956 (1994).
2. M. J. Yin, Y. Yamamoto, R. B. Gaynor, *Nature* **396**, 77 (1998).
3. W. Ebstein, *Berl. Klin. Wochnschr.* **13**, 337 (1876).
4. R. T. Williamson, *Br. Med. J.* **1**, 760 (1901).
5. J. Reid, A. I. Macdougall, M. M. Andrews, *Br. Med. J.* **2**, 1071 (1957).
6. S. G. Gilgore, *Diabetes* **9**, 392 (1960).
7. S. H. Baron, *Diabetes Care* **5**, 64 (1982).
8. Harvested liver and plantaris muscle samples were powdered under liquid nitrogen and homogenized in ice-cold buffer [30 mM Hepes (pH 7.4), 150 mM NaCl, 10% glycerol, 1% Triton X-100, 1 mM phenylmethylsulfonyl fluoride (PMSF), 3 μM aprotinin, 10 μM leupeptin, 5 μM pepstatin A, 25 mM benzamidine, 2 mM sodium orthovanadate, 5 mM β-glycerolphosphate, 100 mM NaF, 1 mM ammonium molybdate, 30 mM tetrasodium pyrophosphate, and 5 mM EGTA] for 30 s with a polytron. After centrifugation, proteins of interest were immunoprecipitated from supernatant solutions, separated by SDS–polyacrylamide gel electrophoresis (SDS-PAGE), and identified by Western blotting. In some cases, immunoprecipitated IRS-1 was treated with alkaline phosphatase (Boehringer-Mannheim; 60 U per 100-μl sample) for 60 min before separation by SDS-PAGE and Western blotting.
9. J. F. Caro, L. G. Dohm, W. J. Pories, M. K. Sinha, *Diabetes Metab. Rev.* **5**, 665 (1989).
10. L. J. Goodyear *et al.*, *J. Clin. Invest.* **95**, 2195 (1995).
11. Supplementary Web material is available on *Science* Online at www.sciencemag.org/cgi/content/full/293/5535/1673/DC1.
12. J. Lee, M. Yuan, L. Hansen, S. E. Shoelson, unpublished data.
13. Murine 3T3-L1 fibroblasts (American Type Culture Collection) were maintained in Dulbecco's modified Eagle's medium (DMEM) containing 25 mM glucose and 10% calf serum under 5% CO_2 in air. Confluent monolayers were differentiated into adipocytes by treatment for 3 days with DMEM containing 10% fetal bovine serum (FBS), insulin (10 μg/ml), 1.0 mM dexamethasone, and 0.5 mM isobutyl-1-methylxanthine under 10% CO_2. Cells were returned to DMEM containing 10% FBS and used for experiments 8 to 13 days after the initiation of differentiation. Before these experiments, differentiated 3T3-L1 adipocytes were serum-starved for 16 hours in DMEM containing 0.1% bovine serum albumin (BSA). Stocks (1.0 M) of acetylsalicylic acid (ASA) in 1.0 M tris-HCL were freshly prepared and pH was corrected to 7.4. Adipocytes were pretreated with 5 or 10 mM ASA for 2 hours at 37°C and then treated with either 6 nM murine TNF-α (mTNF-α) for 20 min, 2 nM calyculin A for 30 min, or 1 nM okadaic acid for 30 min at 37°C. Cells were stimulated with 10 or 100 nM insulin for 5 min at 37°C, washed twice with ice-cold Hepes buffer (25 mM, pH 7.4) containing 10% Earl's balanced salt solution (Gibco) and 0.1% BSA, and solubilized in tris-HCl buffer (50 mM, pH 7.4) containing 0.1% Triton X-100, 0.25% deoxycholate, 150 mM NaCl, 1 mM EGTA, 2 mM sodium orthovanadate, 100 mM NaF, 30 mM pyrophosphate, and freshly added protease inhibitors [1 mM PMSF, trasylol (1 μg/ml), leupeptin (1 μg/ml), and pepstatin (1 μg/ml)]. The cell lysates were clarified; equivalent amounts of proteins were precipitated with antibodies to IR (anti-IR) or antibodies to IRS1 (anti-IRS1) coupled to protein G–agarose, separated by SDS-PAGE under reducing conditions, transferred to PVDF membranes, and detected by immunoblotting with the relevant antibodies: antibody to phosphotyrosine (4G10; anti-pY) or COOH-terminally directed polyclonal anti-IR or anti-IRS1, followed by horseradish peroxidase (HRP)–conjugated second antibody to rabbit. The bands were visualized with enhanced chemiluminescence and quantified by scanning densitometry.
14. M. Karin, M. Delhase, *Semin. Immunol.* **12**, 85 (2000).
15. J. A. DiDonato, M. Hayakawa, D. M. Rothwarf, E. Zandi, M. Karin, *Nature* **388**, 548 (1997).
16. E. W. Harhaj, S. C. Sun, *J. Biol. Chem.* **272**, 5409 (1997).
17. K. A. Robinson, K. P. Boggs, M. G. Buse, *Am. J. Physiol.* **265**, E36 (1993).
18. K. Paz *et al.*, *J. Biol. Chem.* **272**, 29911 (1997).
19. N. Konstantopoulos, S. E. Shoelson, unpublished data.
20. Fao hepatoma cells, grown to 80% confluency, were serum-starved for 16 hours at 37°C in RPMI media containing 0.1% BSA. Stock solutions of 1.0 M aspirin and 1.0 M sodium salicylate were freshly prepared in 1.0 M tris-HCl (pH 7.4); stock solutions of 10 mM ibuprofen, 10 mM naproxen, and 10 mM NS-398 (Biomol, Plymouth, PA) were freshly prepared in ethanol.
21. D. E. Furst, *Arthritis Rheum.* **37**, 1 (1994).
22. *Cox1*$^{-/-}$ or *Cox2*$^{-/-}$ and *Lep*$^{ob/+}$ mice were crossbred to generate *Cox1*$^{+/-}$*Lep*$^{ob/ob}$, *Cox1*$^{-/-}$*Lep*$^{ob/ob}$, *Cox2*$^{+/-}$*Lep*$^{ob/ob}$, and *Cox2*$^{-/-}$*Lep*$^{ob/ob}$ mice (M. Yuan, L. Hansen, S. E. Shoelson, unpublished data).
23. E. Zandi, D. M. Rothwarf, M. Delhase, M. Hayakawa, M. Karin, *Cell* **91**, 243 (1997).
24. Q. Li, D. Van Antwerp, F. Mercurio, K. F. Lee, I. M. Verma, *Science* **284**, 321 (1999).
25. Z. W. Li *et al.*, *J. Exp. Med.* **189**, 1839 (1999).
26. J. C. Pickup, M. A. Crook, *Diabetologia* **41**, 1241 (1998).
27. A. Festa *et al.*, *Circulation* **102**, 42 (2000).
28. C. H. Lang, C. Dobrescu, G. J. Bagby, *Endocrinology* **130**, 43 (1992).
29. G. S. Hotamisligil, N. S. Shargill, B. M. Spiegelman, *Science* **259**, 87 (1993).
30. R. Feinstein, H. Kanety, M. Z. Papa, B. Lunenfeld, A. Karasik, *J. Biol. Chem.* **268**, 26055 (1993).
31. G. S. Hotamisligil, A. Budavari, D. Murray, B. M. Spiegelman, *J. Clin. Invest.* **94**, 1543 (1994).
32. M. E. Griffin *et al.*, *Diabetes* **48**, 1270 (1999).
33. Z. Sun *et al.*, *Nature* **404**, 402 (2000).
34. J. K. Kim *et al.*, *J. Clin. Invest.* **108**, 437 (2001).

35. This manuscript is dedicated to the memory of Shirley Blauner. We thank T. Maratos-Flier for helpful discussions and J. Warram for assistance with statistical analyses. Supported by NIH grants DK51729 (S.E.S.), DK45493 (S.E.S.), and AI43477 (M.K.); a research grant (S.E.S.) and a Mentor-Based Fellowship (M.Y. and N.K.) from the American Diabetes Association; the Cancer Research Institute (Z.W.L.); an American Cancer Society Research Professorship (M.K.); and a Burroughs Wellcome Fund Scholar Award in Experimental Therapeutics (S.E.S.).

12 April 2001; accepted 12 June 2001

Afterimage of Perceptually Filled-in Surface

Shinsuke Shimojo,[1,2]* Yukiyasu Kamitani,[1] Shin'ya Nishida[2]

An afterimage induced by prior adaptation to a visual stimulus is believed to be due to bleaching of photochemical pigments or neural adaptation in the retina. We report a type of afterimage that appears to require cortical adaptation. Fixating a neon-color spreading configuration led not only to negative afterimages corresponding to the inducers (local afterimages), but also to one corresponding to the perceptually filled-in surface during adaptation (global afterimage). These afterimages were mutually exclusive, undergoing monocular rivalry. The strength of the global afterimage correlated to a greater extent with perceptual filling-in during adaptation than with the strength of the local afterimages. Thus, global afterimages are not merely by-products of local afterimages, but involve adaptation at a cortical representation of surface.

Stimuli such as the one shown in Fig. 1A (left) (Varin configuration) induce vigorous perceptual color spreading, or filling-in (*1*–*3*), allegedly indicating some activation-spreading or completion mechanism in the cortical map (*4*–*6*). Fixating this stimulus leads to afterimages of the local inducers, i.e., the Pacmen/wedges or disks (Fig. 1B, left and center). An observer can also see a global afterimage of the perceptually filled-in surface (the large colored rectangle in this case) whose apparent color is complementary to that of the filled-in surface during the adaptation (Fig. 1B, right) as the opponent color theory predicts (*7*). This observation, together with the data reported below, suggests that cortical global processes and their adaptation are critical com-

[1]California Institute of Technology, Division of Biology, Computation and Neural Systems, Pasadena, CA, 91125, USA. [2]NTT Corporation, NTT Communication Science Laboratories, Human and Information Science Laboratory, Atsugi, Kanagawa, 243-0198, Japan.

*To whom correspondence should be addressed. E-mail: sshimojo@its.caltech.edu

ponents in the mechanism that determines the perception.

The global afterimage cannot be attributed to general fuzziness and leaky edges of the afterimage (*8*), because with adaptation to the inner wedge portions alone (without the outer Pacmen), the four parts corresponding to the wedges are separately visible in the afterimage. The global afterimage is distinct from a conventional afterimage. It is visible at a portion that has not been retinally adapted and it corresponds to a perceptually and cortically filled surface (*9*). This is of theoretical interest because an afterimage typically refers to creation of a visible image without presentation of a testing stimulus (*10*) and is believed to arise from either bleaching of photochemical pigments (*11*, *12*) or neural adaptation in the local retinal region (*13*). We tested two hypotheses concerning the mechanism underlying the formation of the global afterimage. (i) In the element adaptation hypothesis, the global afterimage originates from local afterimages formed by photopigment bleaching and/or neural adaptation in the retina. The color of the global afterimage is merely a result of the ordinary filling-in mechanism. In this view, the known retinal negative afterimage is sufficient, and no cortical adaptation is necessary, to induce the global afterimage. (ii) In the surface adaptation hypothesis, the global afterimage is due to adaptation of neural circuits including cortical neurons that represent the filled-in surface during adaptation (*14*).

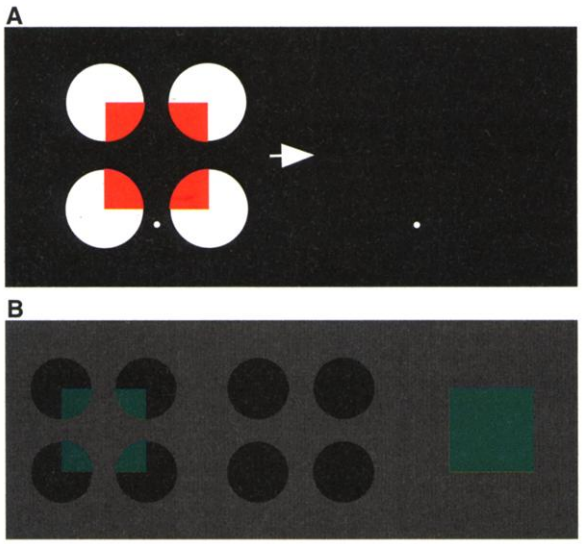

Fig. 1. Afterimages formed by adaptation to the color filling-in configuration. (**A**) The stimuli. (Left) The original Varin configuration for color spreading (filling-in) was used as the adapting stimulus in the first experiment. (Right) Testing. The subject gazed at the fixation point and monitored both the local and the global afterimages on the dark background using two buttons. The reader can observe the afterimages using this display (*7*). The overall size of the stimulus was 8.8° by 8.8°, the disk's diameter was 3.5°, and the fixation point was located 3.1° below the center at the observation distance of 57 cm. Luminance levels of the Pacmen, the wedge portions, and the background were 32.9, 11.9 [red, $(x, y) = (0.62, 0.34)$], and 0.06 cd/m^2, respectively. (**B**) Types of afterimage. (Left and center) Typical local afterimages; (right) the global afterimage. The local afterimages according to our definition included homogeneous disks (center), which were frequently observed, although they may reflect a result of global surface segregation as discussed later. These prototypical afterimages were fully explained to the subjects by illustration before the experiment.

In the first experiment, the subjects fixated and were adapted for 20 s to the Varin configuration (Fig. 1A, left). They then observed the afterimages with a fixation point on a blank screen (Fig. 1A, right) in a semi-dark room. The afterimages typically appeared and disappeared several times during this period. The local and the global afterimages were defined and explained to the observers as the afterimages that corresponded to elements of the inducer (Pacmen, wedges, disks, or their combinations; typical examples are shown in Fig. 1B, left and center) and the image that extended out of them toward the central portion to form a color-filled rectangle (Fig. 1B, right), respectively. The observers monitored the visibility of these types of afterimage separately (*15*). Table 1 summarizes the results. There were significant time periods during which the subjects reported visibility of the global, but not the local, afterimages. They ranged from 8 to 31% of the total observation time across the five subjects tested, with a mean value of 20%. The likelihood of the global afterimage being visible was lower when the local afterimages were visible than when they were invisible. Thus, when the local afterimages of the inducer were visible, the global afterimage tended not to be visible. The same experiment was repeated with other configurations that were known to yield color filling-in, including the Ehrenstein configuration (*16*–*20*). The results were consistent with those of the Varin configuration. The visibility of the local afterimages is neither a necessary, nor even a favorable, condition for that of the global afterimage.

The surface adaptation hypothesis predicts that because the global afterimage is due to the perceptually filled-in surface during adaptation, the strength of the global afterim-

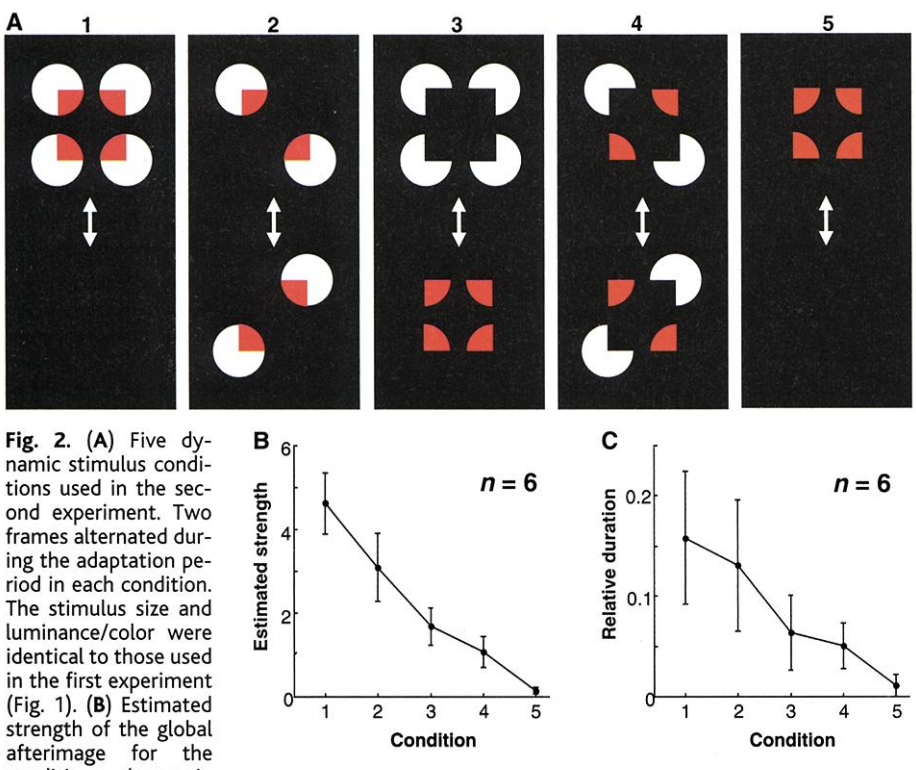

Fig. 2. (**A**) Five dynamic stimulus conditions used in the second experiment. Two frames alternated during the adaptation period in each condition. The stimulus size and luminance/color were identical to those used in the first experiment (Fig. 1). (**B**) Estimated strength of the global afterimage for the conditions shown in (A). The data for six subjects are pooled (error bar, standard error of the mean). The estimated value of 10 corresponds to the strength of the global afterimage for the complete Varin figure (no alternation or decomposition), which had been observed before this experiment. (**C**) Duration of the global afterimage relative to the total test period (40 s) for the conditions shown in (A). The data for six subjects are pooled (error bar, standard error of the mean).

age should be correlated with that of the perceptual filling-in during adaptation (*21*). The element adaptation hypothesis, on the other hand, predicts that the strength of the global afterimage should be determined solely by that of the local afterimages and thus should remain constant as long as the local afterimages are the same. We tested these predictions by dynamically manipulating elements of the inducer during adaptation.

Figure 2A illustrates the adapting stimuli in the second experiment. Two frames of the inducer were alternated, with an equal total duration across portions of the stimulus in all the conditions except for condition 5 (*22*). Consequently, the strength of local afterimages should be the same across conditions 1 to 4 (*23*). The element adaptation hypothesis predicts that the relative strength of the global afterimage would be approximately the same across conditions 1 to 4 (and perhaps weaker in condition 5). Note, however, that the strength of perceptual filling-in during adaptation varies across the conditions, approximately in this rank order (*24*). The surface adaptation hypothesis predicts the strength of the global afterimage to be in this rank order. After adaptation, the subjects estimated the strength of the global afterimage (*25*). Correlation coefficient (Spearman's r) between the rank order of the global afterimage strength and the prediction of the surface adaptation hypothesis ranged from 0.9 to 1.0, and all were individually significant ($P < 0.05$) (Fig. 2B). The consistency across subjects was also highly significant (coefficient concordance $W = 0.84$, $P < 0.005$). In an additional experiment, the subjects monitored the two types of afterimage after adapting to each of the five stimuli in the procedure similar to that in the first experiment. The obtained duration of the afterimage (Fig. 2C) was qualitatively consistent with the estimation results, supporting the surface adaptation hypothesis, but not the element adaptation hypothesis. A spatial structure that can be constructed only at cortical levels determines the strength of the global afterimage.

The final experiment aimed to further dissociate the predictions of the hypotheses. In the static condition (Fig. 3A), the line segments were placed sparsely and statically, so that the impression of color filling-in of the central, disk-shaped region would be minimal, while the local afterimage of the line segments formed strongly. In the dynamic condition (Fig. 3B), the line segments were displaced up and down to create an impression of motion, while the disk-shaped area within which the line segments were colored blue was fixed. It appeared as though a set of white line segments moved up and down behind a semitransparent, stationary colored disk. This condition was designed to enhance the impression of color filling-in maximally during adaptation, while minimizing the local afterimage of line segments by the constant displacement. The surface adaptation hypothesis predicts a dissociation in the dynamic condition: The strength or duration of the local afterimage would be reduced, whereas that of the global afterimage would be increased, relative to the static condition. The element adaptation hypothesis, on the other hand, predicts that both local and global afterimages would be attenuated in the dynamic condition, because the strength of the global afterimage should depend strictly upon that of the local afterimage. The afterimage monitoring procedure was again used. Figure 3B shows the duration of the visible afterimages. The results clearly indicate the dissociation between the two types of afterimages, consistent only with the surface adaptation hypothesis.

The type of afterimage that we describe occupies a region outside the retinally adapted region. The results of our experiments indicate that the global afterimage reflects adaptation of the neural circuits that represent the perceptually filled-in surface during adaptation (surface ad-

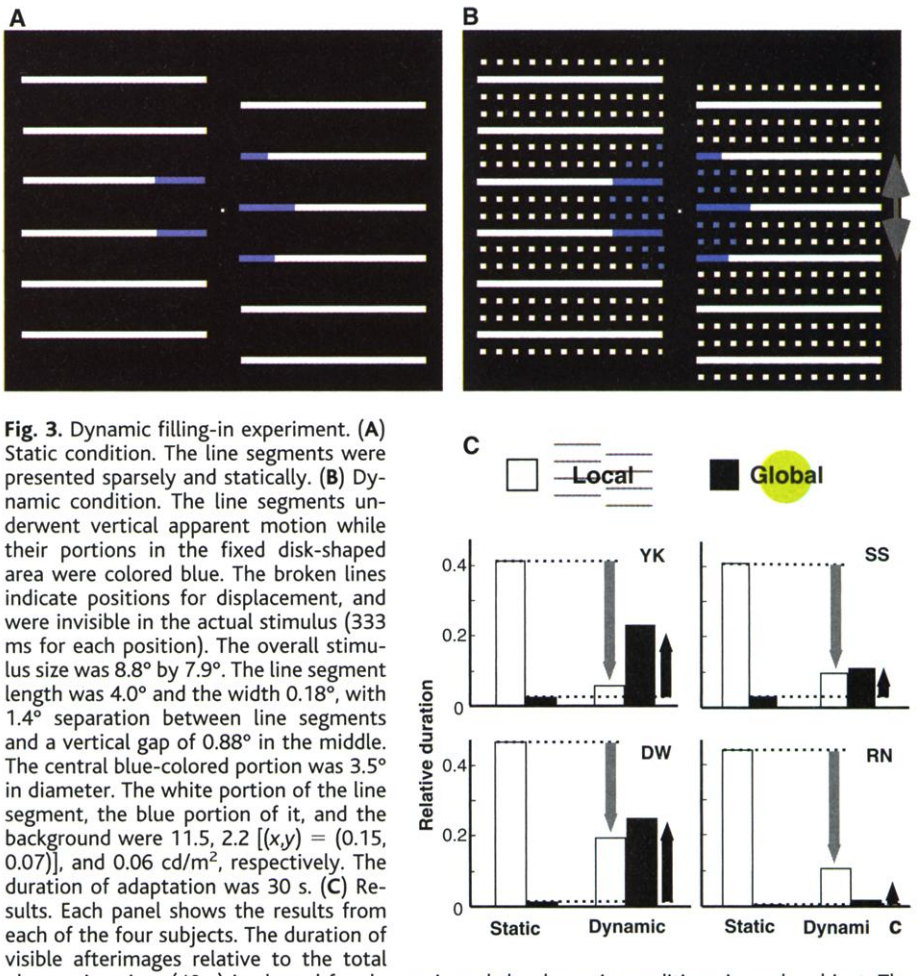

Fig. 3. Dynamic filling-in experiment. (**A**) Static condition. The line segments were presented sparsely and statically. (**B**) Dynamic condition. The line segments underwent vertical apparent motion while their portions in the fixed disk-shaped area were colored blue. The broken lines indicate positions for displacement, and were invisible in the actual stimulus (333 ms for each position). The overall stimulus size was 8.8° by 7.9°. The line segment length was 4.0° and the width 0.18°, with 1.4° separation between line segments and a vertical gap of 0.88° in the middle. The central blue-colored portion was 3.5° in diameter. The white portion of the line segment, the blue portion of it, and the background were 11.5, 2.2 [$(x,y) = (0.15, 0.07)$], and 0.06 cd/m^2, respectively. The duration of adaptation was 30 s. (**C**) Results. Each panel shows the results from each of the four subjects. The duration of visible afterimages relative to the total observation time (40 s) is plotted for the static and the dynamic conditions in each subject. The white and black bars indicate local and global afterimages, respectively.

Table 1. Results of the monitoring experiment. L, G, L&G, and N denote the proportions of the time in which the local afterimage only was visible, the global afterimage only, both, and none of them, respectively.

Subject	Relative duration				Likelihood of global afterimage		
					Given local afterimage		Given no local afterimage
	L	G	L&G	N	L&G/(L&G + L)		G/(G + N)
SS	0.35	0.31	0.19	0.15	0.35	<	0.66
YK	0.43	0.22	0.04	0.31	0.09	<	0.42
JW	0.49	0.25	0.04	0.22	0.07	<	0.53
RN	0.46	0.08	0.10	0.36	0.18	<	0.19
KW	0.58	0.15	0.21	0.06	0.27	<	0.70

aptation hypothesis), as opposed to filling-in induced by the local afterimages during the test period (element adaptation hypothesis). The rivalry between the two types of afterimages (the first experiment) is not consistent even with a compromised notion that the presence of visible local afterimages, as well as the adaptation of cortical neurons, contributes to the formation of the global afterimage. The dissociation of the two types of afterimages was further supported by an additional observation. When the retina was bleached by an intense, flashed adapting stimulus, no or little global afterimage was visible, whereas the local afterimages were vivid and lasted for several minutes. These local afterimages may be due to selective bleaching of photopigments, and possibly adaptation of other types of retinal cells, without affecting cortical neurons.

Other observations that we made were, however, seemingly at odds with the idea that cortical visual representation is critical for the global afterimage. First, interocular transfer of adaptation did not occur to induce the global afterimage in the unadapted eye. Second, when one eye was suppressed by means of a pressure-blinding procedure after adaptation, the global as well as the local afterimages became invisible. These observations indicate an indirect contribution of peripheral adaptation to the perception of the global afterimage. They may imply that the peripheral adaptation (possibly below the visibility threshold), but not the visible local afterimages per se, contributes to the global afterimage. The rivalry between the local and the global afterimages may be considered as suppression between two cortical representations. Input from the adapted retina is thus necessary but not sufficient for perceiving both types of afterimage.

Our findings are consistent with previous studies suggesting that afterimages produced by long exposures to moderate-intensity patterns are not due to photopigment bleaching but rather to neural adaptation (*26–28*), and that the appearance of the afterimage depends on the perceptual, not physical, attribute of the adapting stimulus (*26*, *29*, *30*). Other studies indicate cortical modulation of afterimages created at peripheral levels (*31*, *32*). These studies, however, have not specifically indicated adaptation at a global surface representation that underlies filling-in (*33*). The rivalry between the local and global afterimages may be related to the monocular rivalry reported with patterned ordinary afterimages (*34–37*). Our finding is, however, distinctive in that (i) the rivalry was observed with an afterimage of a perceptually filled-in surface that had not been retinally given, and (ii) the timing (and therefore, the grouping) factor among the elements of the adaptation stimulus was shown to be critical (the second experiment).

When color filling-in occurs, the colored surface is not only completed, but also perceptually segregated from the inducer (*19*, *20*, *38*, *39*). In the Varin configuration (Fig. 1A, left), the four disks and the filled-in rectangular surface appear to be segregated in depth (*40*). These surface representations may undergo adaptation separately and thus lead to corresponding afterimages segregated in time, although the exact nature of the surface representation is unclear. Whereas the global afterimage itself is consistent with the notion of topographical representation with a single-layered, point-by-point map for perceptually filled-in surfaces (*4–6*), this type of representation may not be sufficient to account for the finding that the local and global afterimages spatially overlapped, and yet alternated as two separate chunks in rivalry. Instead, it may indicate symbolic representations of surfaces, which assemble low-level visual representations and control the visibility.

References and Notes

1. D. Varin, *Riv. Psicol.* **65**, 101 (1971).
2. C. Ware, *Perception* **9**, 103 (1980).
3. G. E. Meyer, T. Dougherty, *J. Exp. Psychol. Hum. Percept. Perform.* **13**, 353 (1987).
4. L. Pessoa, E. Thompson, A. Noe, *Behav. Brain Sci.* **21**, 723 (1997).
5. L. Pessoa, H. Neumann, *Trends Cognit. Sci.* **2**, 422 (1998).
6. P. De Weerd, R. Desimone, L. Ungerleider, *Vision Res.* **38**, 2721 (1998).
7. A reader may try observing this by staring at the fixation point in the left panel of Fig. 1A for at least 20 s and then staring at the fixation point in the right panel. Duplicating this test on a cathode ray tube (CRT) display would yield clearer afterimages due to higher luminance/contrast (the same stimulus is available at http://neuro.caltech.edu/~kamitani/fillingInAfterimage). Different portions of afterimages may appear and disappear several times at different intervals.
8. D. H. Kelly, E. Martinez-Uriegas, *J. Opt. Soc. Am.* **A10**, 29 (1993).
9. Neon color spreading created by dichoptically presenting the Ehrenstein configuration has been reported (*41*). Long-range contour interactions and figure-ground segregation characterize cortical, as opposed to subcortical, processes (*42*, *43*).
10. This is in contrast to visual aftereffects, which usually refer to perceptual modulation of a physically presented testing stimulus due to some cortical adaptation (*44*).
11. G. S. Brindley, *J. Physiol.* **164**, 168 (1962).
12. K. J. W. Craik, *Nature* **145**, 512 (1940).
13. V. Virsu, *Med. Biol.* **56**, 84 (1962).
14. This hypothesis does not exclude the possibility that peripheral adaptation along with cortical adaptation contributes to the formation of the global afterimage, as will be discussed later.
15. The visual stimuli were presented on a CRT monitor controlled by a personal computer (PowerMac 7600). The observers were instructed to press one (the other) of two buttons as soon as the local (global) afterimages appeared, and to release it when they disappeared. The total observation time of 40 s (two 20-s sessions) was divided into four categories with regard to the visibility of the afterimages: (L) local afterimage only, (G) global afterimage only, (L&G) both visible, and (N) neither visible. To analyze time-line contingency between the local and the global afterimages, we calculated the likelihood of seeing the global afterimage given that the local afterimage was visible or invisible.
16. H. F. J. M. van Tuijl, *Acta Psychol.* **39**, 441 (1975).
17. C. Redies, L. Spillman, *Perception* **10**, 667 (1981).
18. C. Redies, L. Spillman, K. Kunz, *Vision Res.* **24**, 1301 (1984).
19. K. Nakayama, S. Shimojo, V. S. Ramachandran, *Perception* **19**, 497 (1990).
20. K. Nakayama, S. Shimojo, *Science* **257**, 1357 (1992).
21. The results of a separate experiment to directly examine this correlation were consistent with the prediction (*45*). Luminance contrast across portions of the adapting stimulus was manipulated in this experiment.
22. Each of the alternating frames was 667 ms, and the total duration of adaptation was 13.4 s (10 cycles). Condition 5 did not include the Pacman portions of the stimulus at all and thus had only half the total duration of the other four conditions.
23. However, the afterimage is generally weaker after adapting to on-off stimuli (*28*, *30*).
24. Conditions 1 and 2 lead to color filling-in, although only partial in time (1) or space (2); conditions 3 and 4 lead to very little color filling-in, but an illusory contour and appropriate surface segregation may be available; condition 5 does not have any of these factors.
25. The subject performed estimation by adjusting the position of a cursor on a scale on the display. The five conditions were randomized and repeated three times in a session of 15 trials. For each of the six subjects tested, the rank order among the conditions was determined on the basis of the mean estimates. Correlation coefficient (Spearman's r) between the rank order in each subject and the prediction of the surface adaptation hypothesis was calculated.
26. J. M. Loomis, *Vision Res.* **12**, 1587 (1972).
27. V. Virsu, P. Laurinen, *Vision Res.* **17**, 853 (1977).
28. J. M. Loomis, *J. Opt. Soc. Am.* **68**, 411 (1978).
29. F. Shively, *Percept. Psychophys.* **13**, 525. (1973).
30. S. Anstis, B. Rogers, J. Henry, *Vision Res.* **18**, 899 (1978).
31. P. Davies, *Br. J. Psychol.* **64**, 325 (1973).
32. M. M. Hayhoe, D. R. Williams, *Perception* **13**, 455 (1984).
33. See Ramachandran and Gregory (*46*) for a possible exception, although this is a quite peculiar case where a dynamic afterimage is observed.
34. J. Atkinson, *Percept. Psychophys.* **12**, 257 (1973).
35. F. Sindermann, H. Lueddeke, *Vision Res.* **12**, 763 (1972).
36. J. Atkinson, *J. Exp. Psychol.* **98**, 55 (1972).
37. B. Crassini, J. Broerse, *Vision Res.* **22**, 203 (1982).
38. K. Nakayama, Z. J. He, S. Shimojo, in *An Invitation to Cognitive Science*, D. N. Osherson, Ed., vol. 2, *Visual Cognition*, S. M. Kosslyn, D. N. Osherson, Eds. (MIT Press, Cambridge, MA, 1998), pp.1–70.
39. Another way to manipulate the surface and color filling-in properties during adaptation would be to add binocular disparity to the wedge portions (*19*). Although our preliminary observations were consistent with the prediction of the surface adaptation hypothesis, the effects of binocular disparity were generally weak and turned out not to be decisive. The weak effects may be due to either easy breakdown of the stereo perception as a result of prolonged fixation (according to the surface adaptation hypothesis) or to fuzziness of binocular disparity in the afterimages themselves (according to the element adaptation hypothesis). Similarly, one can have a faint impression of a global afterimage after adaptation to a dichoptically constructed Ehrenstein or Varin configuration. This may be considered as another line of evidence in favor of the surface adaptation hypothesis, although the effect is weak.
40. See http://neuro.caltech.edu/~kamitani/fillingInAfterimage.
41. H. Takeichi, S. Shimojo, T. Watanabe, *Perception* **21**, 313 (1992).
42. C. D. Gilbert, A. Das, M. Ito, M. Kapadia, G. Westheimer, *Proc. Natl. Acad. Sci. U.S.A.* **93**, 615 (1996).
43. V. A. F. Lamme, *J. Neurosci.* **15**, 1605 (1995).
44. G. Mother, F. Verstraten, S. Anstis, Eds., *The Motion Aftereffect* (MIT Press, Cambridge, MA, 1998).
45. S. Shimojo, Y. Kamitani, *Neurosci. Abstr.* 1053 (1999).
46. V. S. Ramachandran, R. L. Gregory, *Nature* **350**, 699 (1991).

47. We thank L. Shams and B. Sheth for helpful comments, and S. Z. Smith for editorial assistance. Supported by Califomia Institute of Technology and NTT Communication Science Laboratories.

23 February 2001; accepted 15 June 2001